Chinese Chemical Letters 36 (2025) 110374

Contents lists available at ScienceDirect

Chinese Chemical Letters

journal homepage: www.elsevier.com/locate/cclet

Design and engineering strategies of porous carbonaceous catalysts toward activation of peroxides for aqueous organic pollutants oxidation

Bofeng Li[a], Yuxian Wang[a,*], Ya Liu[b], Zhe Han[a], Tiantian Xing[a], Yumin Zhang[a], Chunmao Chen[a,*]

[a] State Key Laboratory of Heavy Oil Processing, China University of Petroleum-Beijing, Beijing 102249, China
[b] School of Chemical Engineering, The University of Adelaide, Adelaide, SA 5005, Australia

ARTICLE INFO

Article history:
Received 13 May 2024
Revised 22 July 2024
Accepted 25 August 2024
Available online 26 August 2024

Keywords:
Porous carbocatalysts
Advanced oxidation processes (AOPs)
Peroxide activation
Pore construction
Activity tuning

ABSTRACT

Advanced oxidation processes (AOPs) governed by peroxide activation to produce highly oxidative active species have been extensively explored for environmental remediation. Nevertheless, the low diffusion rates, inadequate interactions of the reactants, and limited active site exposure hinder treatment efficiency. Porous carbocatalysts with high specific surface area, tunable pore size, and programmable active sites demonstrate outstanding performance in activating diverse types of peroxides to generate active species for treatment of aqueous organic pollutants. The pore-rich structures enhance reaction kinetics for peroxide activation by facilitating diffusion of the reactants and their interactions. Additionally, the structural flexibility of porous structures favors the accommodation of highly dispersed metal species and allows for precise tuning of the microenvironment around the active sites, which further enhances the catalytic activity. This review critically summarizes the recent research progress in the applications of engineered porous carbocatalysts for peroxide activation and outlines the prevailing pore construction methods in carbocatalysts. Moreover, engineering strategies to regulate the mass transfer efficiency and fine-tune the microenvironment around the active sites are systematically addressed to enhance their catalytic peroxide activation performances. Challenges and future research opportunities pertaining to the design, optimization, mechanistic investigation, and practical application of porous carbocatalysts in peroxide activation are also proposed.

1. Introduction

The rapid industrialization and urbanization have been deteriorating the environment. Emerging organic pollutants such as pharmaceutical and personal care products, and industrial chemicals are continuously being released into the aquatic environments [1,2]. These persistent organic pollutants pose a danger to nature lives because of their high toxicities and resistance to degradation. Moreover, they might ultimately enter the human body through bioaccumulation, posing a significant threat to human health [1]. Advanced oxidation processes (AOPs), especially heterogeneous activation of the peroxides such as hydrogen peroxide, persulfates, ozone, percarbonates, and peracetic acid, have been demonstrated to effectively to oxidize these organic pollutants. The activation of peroxyl bonds within the peroxides can generate highly oxidative active species that mineralize the organic pollutants or convert them into low-toxic, value-added polymers [3].

Transition metal oxides exhibit high catalytic activities for peroxide activation [4]. The highly overlapped 3d orbitals of transition metals and the O 2p orbitals of peroxides facilitates the transfer of free electrons from transition metals to peroxyl bonds, thereby promoting peroxide activation to generate oxidative reactive oxygen species (ROS) [5]. However, bulk-form transition metal oxides suffer from the inadequate exposure of active sites, which hinders sufficient interactions of the reactants [6]. Additionally, metal leaching during the reaction poses another critical challenge [7]. The resulting secondary pollution might lead to more severe environmental issues than the primary one. Over the past decade, carbocatalysts with controllable porous structures and programmable active sites have attracted intensive research interests in peroxide activation [8,9]. The great structural tunability of the carbocatalysts enables the creation special spaces to enhance reaction kinet-

* Corresponding authors.
E-mail addresses: yuxian.wang@cup.edu.cn (Y. Wang), c.chen@cup.edu.cn (C. Chen).

https://doi.org/10.1016/j.cclet.2024.110374
1001-8417/

ics [10]. Additionally, the created pore structures can also facilitate the accommodation of metal species, prevent nanoparticles from aggregation, and ensuring a high distribution of active sites [11].

Pore structures within carbocatalysts are of vital significance to affect their catalytic performances in peroxide activation. They influence not only the adsorption capacity of carbocatalysts, but also the mass transfer and even reaction thermodynamics during peroxide activation [12,13]. Pore size tuning, wettability control, and defect engineering are the prevailing strategies to regulate the pore properties [14-16]. The construction of meso/macroporous structures enhances the specific surface area (SSA) of the carbocatalysts and facilitates the diffusion of the reactants within the carbocatalysts [17]. Moreover, the induced nanoconfinement effect in mesopores boosts the reaction kinetics by enhancing the mass transfer rates and regulating the molecular behaviors of the reactants [10]. Wettability control is critical for tuning interactions between reactants and the surface of carbocatalysts [18]. Studies revealed that increasing the hydrophilicity benefits di-phase reaction systems, while developing a gas diffusion layer (GDL)-based diffusion interface promotes the mass transfer in tri-phase systems [19]. Defect engineering, through defect introduction and heteroatom doping, optimizes the microenvironment around the active sites and modulates the electronic properties of the carbon matrix, thereby enhancing catalyst-peroxide interactions [20].

To date, reviews on applications of porous carbonaceous materials as the heterogeneous catalysts in the fields such as energy storage, energy conversion, and environmental remediation have been reported [21,22]. However, faced with the limitations such as low diffusion rates and inadequate interactions of the reactants, and insufficient exposure of the active sites in AOPs, there is still lack of a review that systematically summarizes the synthesis, optimization, and application of the engineered porous carbocatalysts toward the effective activation of the peroxides for oxidation of the aqueous organic pollutants. This review starts by introducing the prevailing pore construction methods in carbocatalysts. Engineering strategies for regulating mass transfer efficiency and tuning the microenvironment around the active sites are then systematically outlined, which help enhance the activities of porous carbocatalysts in peroxide activation. Moreover, this review critically summarized the applications of the engineered porous carbocatalysts in activation of different types of peroxides. Lastly, challenges and future research opportunities in peroxides activation by porous carbocatalysts are proposed.

2. Pore structure construction

Pore structures in carbonaceous catalysts significantly affect their mechanical strength, electronic properties, mass transfer ability, and chemical stability [16]. Additionally, pores may serve as crucial sites for anchoring heteroatoms and heteroparticles, favoring the adsorption of the peroxides and the subsequent dissociation of their peroxyl bonds to produce ROS production. The International Union of Pure and Applied Chemistry (IUPAC) classifies pores into micropores (<2 nm), mesopores (2–50 nm), and macropores (>50 nm) based on size [23]. Micropores ensure high dispersion of anchored metal atoms or nanoparticles, effectively preventing aggregation [11]. However, the small size of micropores and the relatively long inter-pore spacing may hinder the efficient diffusion of reactants, impeding reaction kinetics. Mesopores facilitate the rapid transport of reactants and solvents and the reported nanoconfinement effects which boost the interactions between the reactants by enriching their concentrations and altering the reaction thermodynamics are mostly observed in mesoporous structures [24]. Macropores interconnect the bulk phase of the catalysts. The macroporous carbonaceous skeleton also favors the formation of hybrid structures with other materials [25]. Therefore, the constructing pore structures and regulating their size and distribution are critical to optimize the activities of carbocatalysts [14]. The following figure summarizes the strategies for constructing various pores and regulating their sizes (Fig. 1). Additionally, some detailed features of these pore-forming strategies such as properties, advantages, disadvantages, and application fields as listed in Table S1 (Supporting information).

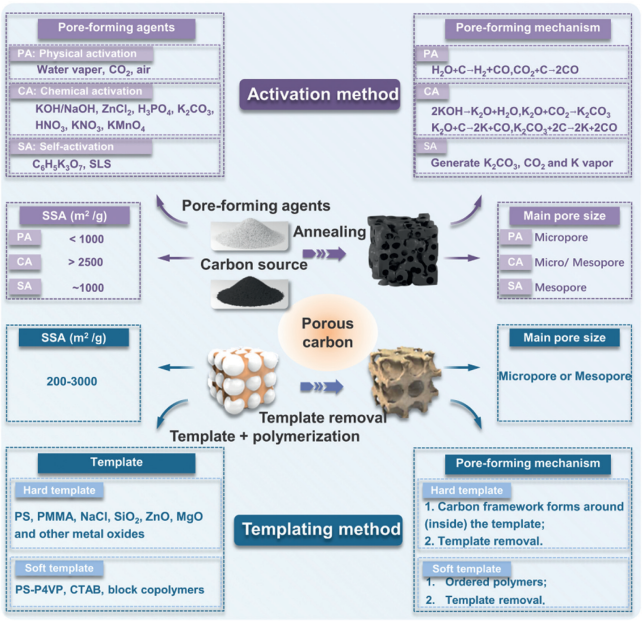

Fig. 1. Strategies for constructing different pores and regulating their sizes.

2.1. Physical/chemical activation method

Physical and chemical activations are widely employed to create pores in carbonaceous materials *via* etching. In a typical physical activation (PA) process, carbon precursors are firstly carbonized, and then activating agents such as water vapor, carbon dioxide, or air introduced at elevated temperatures activate the carbonized precursors [26]. It has been reported that micropores are the predominant pores formed through physical activation [27]. Chemical activations (CA) rely on the etching and oxidation effects of the added chemical reagents or their decomposition products at high temperature. Commonly used chemical reagents include KOH/NaOH, $ZnCl_2$, H_3PO_4, K_2CO_3, HNO_3, and $KMnO_4$ [28-30]. These agents react chemically with carbon materials and influence the pyrolysis process, enhancing the pore formations. Notably, the added oxidative reagents, such as HNO_3, KNO_3, and $KMnO_4$, can penetrate the carbon precursors and oxidize their inner structures [29,30]. Compared to physical activations, chemical activations yield porous structures with distinct pore size distributions [29]. Wang *et al.* utilized KOH as the pore-forming agent to create pores on asphalt powder-based graphitic carbon. The rich microporous structures enlarged specific surface area of the as-obtained porous carbon to 3002 m^2/g [31]. Micropores ranging from 0.4 nm to 1.9 nm were successfully created in single-walled carbon nanohorns (SWNHs) with nitric acid treatment [32]. Additionally, the decomposition products of $KMnO_4$ at high temperatures such as K_2MnO_4, MnO_2, and O_2 can etch the carbon framework and assist the formation of mesoporous structures [33].

Apart from the externally added chemicals, decomposition citrate ($C_6H_5K_3O_7$), sodium lignosulfonate (SLS) and sodium tartrate at high temperatures can also etch or oxidize the formed carbonized structure [34-36]. The environmentally benign and

cost-effective behaviors render this self-activation (SA) process a promising technique with broad applications. For example, high-temperature pyrolysis of $C_6H_5K_3O_7$ can produce microporous carbons featuring excellent SSAs by the generated K_2CO_3, CO_2 and potassium vapor. However, narrow microporous size distributions and low pore volumes are often expected by high temperature $C_6H_5K_3O_7$ pyrolysis, hindering the rapid diffusion of the reactants [37].

2.2. Templating method

The template method is widely used to construct ordered porous carbon materials, where pore structures are formed by removing the template, often mirroring the size of the templates [38]. Therefore, pore diameters can be tuned by altering the size/concentration of the template. According to the types of templates used, this method can be categorized into hard and soft templating approaches [38-40]. The hard templating approach employs pre-prepared porous materials or nanocrystals with relatively rigid structures as templates, such as polystyrene (PS) [41], polymethylmethacrylate (PMMA) [42], chloride salts [43], silica spheres [44], metal oxides [45,46], and zeolite molecular sieves [47]. Certain hard templates, like PS, PMMA, and zinc oxide, can be directly removed through high-temperature annealing. Nitrogen-doped carbon nanotubes were synthesized using zinc oxide nanorods as sacrificial templates, in which zinc oxide vaporized during the carbonization process at 900 °C [48]. Nevertheless, removing templates such as silica and zeolite molecular sieves often requires acid or alkali treatment. Moreover, the complexities for the preparation and the removal of such templates, along with the possibly altered physicochemical properties of the carbon surface after chemical etching bring challenges to further applications. With melting points above 750 °C, water-soluble chloride salts can retain their morphology during high-temperature annealing, enabling them as the promising hard template for constructing mesoporous and macroporous structures [49,50]. Chen *et al.* mixed carbon precursors with the sodium chloride solution *via* freeze drying and obtained porous carbon with graphene-like ultrathin and mesoporous walls by high temperature annealing followed by water washing [51].

Unlike hard templates, soft templates refer to ordered polymers by weak intermolecular or intramolecular interactions, such as colloidal particles, microemulsions, vesicles, and lipid nanotubes [52]. Templating agents can form micelles in solution at certain concentrations, guiding the growth of precursors into specific shapes. Additionally, soft templates can be removed by solvent washing, heat treatment, or chemical etching [53,54]. The self-assembly of the positively charged cetyltrimethylammonium bromide (CTAB) and negatively charged phenolic resin *via* electrostatic interactions is a well-established strategy to synthesize ordered mesoporous carbon materials [52]. Block copolymers, which consist of two or more covalently bonded copolymers are another type of the soft template. Previous studies have employed block copolymers as soft template to construct ordered structures such as spheres, cylinders, lamellae, and hierarchical assemblies [55]. For example, Mai *et al.* using a simple polystyrene-*block*-poly(ethylene oxide) (PS-*b*-PEO) di-*block* copolymer as the structure-guiding agent to synthesize mesoporous silica with a shifted double diamond (SDD) structure [17]. Employing soft templates to prepare porous carbonaceous catalysts is straightforward and cost-effective, yet controlling the pore size structure of the final product is challenging because of the fluidity of the soft template [56]. Furthermore, improper template removal conditions may impact the microstructure of material, resulting in pore collapse and surface properties damage, and thus affecting the catalytic performance [57]. Wang *et al.* reported the synthesis of Ag hollow spheres by using direct emulsion templating method using beeswax and CTAB solution [58]. The heat treatment temperature to remove the beeswax-based spherical template should be precisely controlled because of its low phase-transformable temperature (~70 °C). Additionally, ethanol was employed as the washing solvent instead of water to ensure the high dissolution of beeswax. The accurate regulation calcination temperature to remove CTAB as the soft template is also critical for the synthesis of mesoporous MnO_2 [59]. It is found that pore structures as well as the crystal phase of MnO_2 were remained when calcination temperature was lower than 400 °C. When calcination temperature exceeded 600 °C, the pores collapsed and the crystal phase of MnO_2 changed to Mn_2O_3/Mn_3O_4, which decreased the capacitance performance. Therefore, careful selection of washing solvents and chemical etchants, along with and precise control of heat treatment conditions, are imperative during the removal of soft templates.

3. Tuning the activities of porous carbonaceous catalysts in peroxide activation

3.1. Pore size regulation

In carbon-driven peroxide activation for the degradation of aqueous organics, the molecular sizes of aqueous organic pollutants commonly range from 0.6 nm to 1.2 nm [60,61]. To ensure a fast mass transfer rate and facilitate the interactions between the produced ROS and the organic pollutants, regulating the pore size of vital significance. As shown in Fig. 2a, micropores smaller than 2 nm greatly impede the diffusion of reactants, potentially impacting the efficiency of peroxide bond activation. Furthermore, the generated ROS from peroxyl bonds dissociation, with short lifetimes (half-lives: $SO_4^{\bullet-} = 30-40$ μs, $^{\bullet}OH = 20$ ns) and limited diffusion distance (approximately 20 nm), struggle to escape from the inner active sites to the bulk solution [62-64]. Macropores provide diffusion channels for reactants to enhance the mass transfer efficiency, yet the oversized pores result in a low density of the exposed active sites on the catalysts. Additionally, large pore structures are difficult to enrich the reactants. Mesoporous materials, with pore sizes ranging from 2 nm to 50 nm, can accommodate and stabilize large molecules, providing an ideal environment for peroxyl bond activation [65]. However, the randomly sized and uneven distributed mesopores may restrict the efficacy in diffusion and adsorption.

Within a certain range of the mesoporous sizes, the physicochemical properties (*e.g.*, density, solubility, reactivity, and catalytic activity) of reactants, along with the mass transfer efficiencies within the space, can undergo significant alternations. This phenomenon is known as the nanoconfinement effect [17]. The nanoconfinement effect in porous carbon catalysts effectively enhances the adsorption of reactants and improves the concentrations of local pollutants. Mesopores function as nanoreactors to enrich and restrict movement of the reactants. The increased collision probability of the reactants boosts the reaction efficiency of short-lived ROS near the catalyst surface [65]. Additionally, the confined space within the mesopores might also change the reaction thermodynamics by influencing the ROS generation routes and oxidation pathways of the organics [10]. As a result, enhanced oxidation efficiency of the aqueous organic pollutants can be expected because of the promoted reaction kinetics and the regulated reaction pathways.

There are other factors influencing the occurrence of the nanoconfinement effect apart from the proper pore size. The mass transport, in particular diffusion and migration of the reactants from the bulk solution to the reaction interfaces on the catalysts is critical in nanoconfinement effect [12,13]. The electrostatic forces between the reactants/reaction intermediates and the cata-

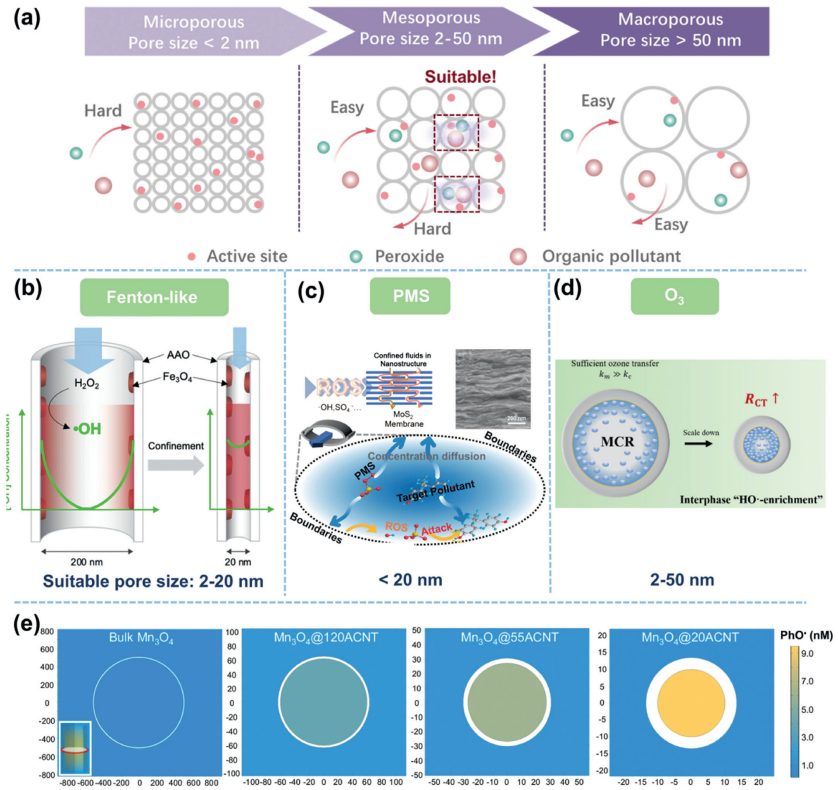

Fig. 2. (a) Schematic illustration of effect of pore size on reaction kinetics. Optimal pore size for occurrence of nanoconfinement effect in different reaction systems: (b) Fenton-like reaction. Reprinted with permission [70]. Copyright 2020, American Chemical Society. (c) PMS activation. Reprinted with permission [62]. Copyright 2019, Wiley-VCH. (d) O_3 activation. Reprinted with permission [75]. Copyright 2018, American Chemical Society. (e) The computed concentration disstribution of PhO• in the mid-section of tubes in different oxidation systems at 50% PhOH conversion. Reprinted with permission [74]. Copyright 2024, Nature.

lysts which are governed by the local charge distributions within the porous structures, ionic states of the reactants, and the ionic strength of the bulk reaction solution affect the efficiency of the mass transportations of the reactants and determine the successful entrance of the reactants within the pore structures [66,67]. Additionally, the steric hinderance within the pore structures and the existence of the natural organic matters in actual wastewater might also influence of the efficacy of nanoconfinement effect [68]. These as-mentioned factors might in turn affect the optimal pore sizes. In future studies, in-depth investigations on the mass transport of the reactants and their electronic interactions with the porous catalysts as well as the influence of the water matrix factors can be performed by both experimental and theoretical analyses are required to unveil origin of the nanoconfinement effect. Machine learning based on the well-developed database can also be used to predict the key factors governing the nanoconfinement effect.

The optimal pore size range for inducing effective nanoconfinement effects varied across various peroxide activation systems because of the distinct reaction mechanisms and mass transfer requirements. For activation processes involving gas-phase oxidants, for example, heterogeneous catalytic ozonation process, the optimal pore size for inducing the nanoconfinement effect is usually larger than that of the diphase Fenton-like activation processes (liquid-solid) because the involvement of gas bubbles requires a larger space to enrich the oxidants [69]. Large pores in catalytic ozonation ensure contact between ozone molecules and the catalyst surface. However, excessively large pores reduce nanoconfinement, affecting ozone decomposition and pollutant oxidation efficiency. In addition, the optimal pore size that maximizes the efficacy of the nanoconfinement effect can be also governed by the factors such as electrostatic forces between the reactants/reaction intermediates and the catalysts, steric hinderance, and the background substances in wastewater besides the types of the activation processes. Therefore, the optimal pore size range might be different even for the same activation process [68].

In Fenton and Fenton-like reactions, the nanoconfinement effect was observed with pore sizes <20 nm (Fig. 2b). Compared with the scenarios occurred in macropores (200–300 nm), mesopores with diameters <20 nm hindered the diffusion of •OH. The notably increased concentration of •OH (from 0.036 pmol/L to 44.6 pmol/L) enhanced its interactions with organic pollutants [70]. Small pores in Fenton-like reactions enhance efficiency by ensuring close contact between metal ions and H_2O_2. In catalytic persulfate activation, the optimum pore size range to induce the nanoconfinement effect has been reported to be between 2 nm and 20 nm (Fig. 2c) [62,71,72]. Moderate pores in peroxymonosulfate (PMS) activation enriched pollutants and the produced ROS in the confined microenvironment induce intensive collisions [73]. Recently, Mn_3O_4 confined in amorphous carbon nanotubes (ACNTs) with varied diameters (Mn_3O_4@nACNT, where n represents the diameter of ACNTs) were synthesized *via* a templating method to initiate nanoconfined heterogeneous PMS activation [74]. Effective diffusion coefficients of phenoxy radical (PhO•) molecules in 20, 55, 120, and 1000 nm pores were calculated to be 5.47, 6.86, 7.44, and 7.95×10^{-10} m^2/s, respectively [74]. The reduced diffusion efficiency enriched PhO•, thereby accelerating oligomer formation, and consequently increased phenol removal in comparison to macropores (Fig. 2e). Studies on catalytic ozonation treatment for recalcitrant organic pollutants have linked catalytic activity with porosity, where a high pore volume of mesopores and large pores in activated carbon, which allows for rapid mass transfer and provides numerous active sites, confers significant advantages to the catalytic process [75,76]. Moreover, it is found that the R_{ct} value

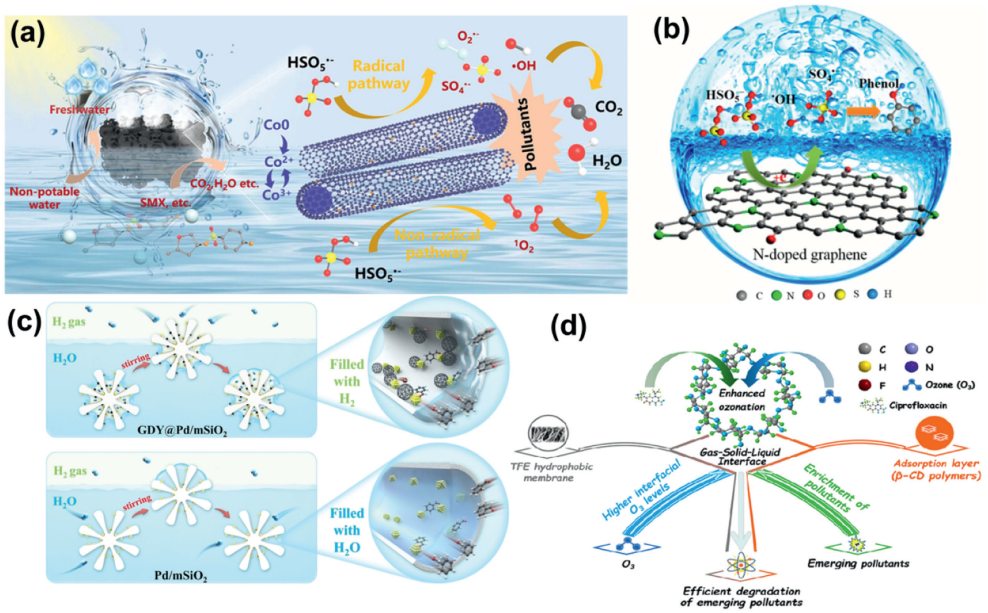

Fig. 3. Enhancement of wettability in liquid-solid systems: (a) Mechanism of catalytic degradation of the CNG-800/MF. Reprinted with permission [77]. Copyright 2023, American Chemical Society. (b) Mechanism of PMS activation and phenol oxidation on N-doped graphene. Reprinted with permission [69]. Copyright 2015, American Chemical Society. Enhancement of wettability in gas-liquid-solid systems. (c) Schematic illustration of the reactions occurring on hydrophobic modified 20GDY@Pd/mSiO_2 and hydrophilic Pd/mSiO_2. Reprinted with permission [79]. Copyright 2022, Wiley-VCH. (d) Schematic illustration of enhancing the ozonation efficiency of a tri-phase system. Reprinted with permission [81]. Copyright 2021, The Royal Society of Chemistry.

(ratio of •OH to O_3 exposure) was enhanced to 8.0×10^{-5} in 10 nm nanochannels due to the confinement in heterogeneous catalytic ozonation, >24 times the rate observed in 168 nm nanochannels (Fig. 2d) [75]. However, precisely enriching reactants within nanoconfined spaces, rather than on external surfaces, remains a technical challenge. Regulating interactions by enhancing electrostatic attraction and tuning wettability is critical for promoting mass transfer efficiency.

3.2. Wettability control

The wettability of the catalysts plays a crucial role in their catalytic performance by affecting mass transfer abilities at the multiphase interfaces. Recently, wettability control has emerged as a key research focus in the heterogeneous peroxide activation processes involving liquid-solid or gas-liquid-solid phase [77,78]. In liquid-solid di-phase systems such as Fenton and Fenton-like reactions, the wettability of the catalysts is the key to determine the interactions of aqueous solution containing both peroxides and organics with the surface of the catalysts, in which high hydrophilicity favors the uniform dispersion of the aqueous solution (Fig. 3a) [77]. Metal-free heteroatom doping and surface modifications are two common strategies used to regulate the hydrophilicity of the porous carbonaceous catalysts. Adjusting the types and concentrations of N-doping and can regulate the wettability of the carbonaceous catalysts as the lone-pair electrons in the doped N atoms alter the surface charge distribution and influence the electrostatic force interaction with water molecules (Fig. 3b) [69]. Moreover, hydrogen peroxide treatment has been used to enhance the hydrophilicity of mesoporous carbon loaded with iron oxide nanoparticles (Fe/meso–C). The increased hydrophilicity enables the well dispersion of Fe/meso–C in the reaction solution, facilitating the rapid mass transfer for fast degradation of methylene blue [15].

In gas-liquid-solid tri-phase reactions, besides adjusting the hydrophilicity, tuning the hydrophobicity/aerophilicity of the catalysts is equally important because of the presence of the gas phase reactants (Fig. 3c) [79]. Using the tri-phase heterogeneous catalytic ozonation (HCO) system as an example, both ozone and organic pollutant molecules exhibit strong affinities towards hydrophobic surfaces, while the organic pollutant molecules need to be dissolved into reaction solution to reach surface active sites and react with the generated •OH in the aqueous phase, which can be facilitated by the hydrophilic surface. However, making catalysts exhibit both strong hydrophilicity and hydrophobicity is challenging. Furthermore, the limited solubility of O_3 in water (525 mg/L at 298 K) and its poor diffusion coefficient (1.85×10^{-5} cm^2/s at 298 K) in the liquid phase impede the mass transfer efficiency [80]. Constructing a tri-phase mass transfer interface by loading hydrophilic catalysts onto a hydrophobic gas diffusion layer (GDL) is a promising strategy to enrich aqueous organic pollutants, quickly transfer O_3, and enhance catalytic ozonation efficiency. Given that the diffusion coefficient of O_3 in the gas phase is orders of magnitude higher than that in the liquid phase, O_3 can be directly introduced to the side of GDL without catalyst loading [81,82]. The reaction solution can be fed to the side with catalyst loading to enhance the hydrophilic interactions. Studies have revealed that the gaseous reactants could maintain high concentrations near the GDL [19]. Moreover, gaseous reactants have a diffusion distance of around 50 nm at the tri-phase GDL interface, significantly less than the 50 μm found at conventional interfaces [82]. The rapid consumption of the gaseous O_3 in turn drives the quick mass transfer rate through GDL. As a result, the formed gas−solid−liquid tri-phase reaction interface can boost the chemical reactions by accelerating the reaction kinetics. In a recent study, Wang *et al.* synthesized hydrophilic cross-linked β-cyclodextrin polymers (CDPs) and loaded them onto the hydrophobic polytetrafluoroethylene (PTFE) membrane as the GDL to construct the gas−solid−liquid tri-phase reaction interface [81]. The improved interface adsorption ability of the aqueous pollutants and the enriched O_3 concentrations at the reaction interface accounted for the high pollutant's removal efficiency and fast reaction kinetics (Fig. 3d).

3.3. Defect engineering

Pristine carbonaceous materials often exhibit poor catalytic activities because of the uniformly distributed surface charge den-

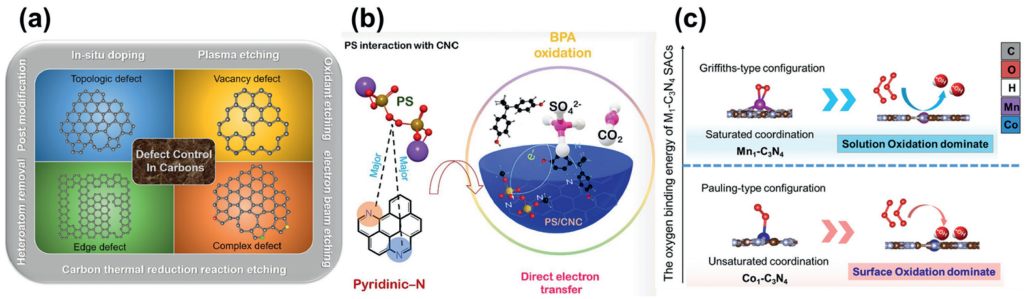

Fig. 4. (a) Synthetic methodology of carbon-based defects. Reprinted with permission [84]. Copyright 2021, Elsevier. (b) Schematic illustration of pyridinic N sites for enhancing the BPA removal efficiency. Reprinted with permission [90]. Copyright 2023, Elsevier. (c) Schematic diagram of the activation mechanism of O_3 over Mn_1–C_3N_4 and Co_1–C_3N_4. Reprinted with permission [96]. Copyright 2022, American Chemical Society.

sity. Surface defect engineering by creating structure/edge defects and/or introducing heteroatoms within the carbon framework can alter the charge distribution and disrupt the chemical inertness of the pristine carbon [83]. Structural and edge defects are comment defects existing in carbocatalysts stemming from the irregular arrangement of C atoms in the graphitic lattice and the dangling bonds at the edge, respectively [16]. These defects compromise the structural integrity of the graphitic lattice and disrupt the conjugated π-network, leading to localized electronic regions [83]. The biased charge distribution of the C atoms at structural and edge defects promotes the adsorption of peroxides and their subsequent activation [16]. Advanced techniques such as *in situ* doping, plasma etching, oxidation etching, electron beam etching, carbon thermal reduction reaction etching, heteroatom removal and post modification, along with ion injection techniques, have been employed for introducing and engineering defects within carbon-based materials (Fig. 4a) [84].

Introducing metal-free heteroatoms (such as B, N, F, P, or S) into the carbon framework triggers a redistribution of surface charge density because of the significant differences in electronegativity and atomic radius between these heteroatoms and carbon atoms [5]. These heteroatom dopants and their adjacent C atoms with altered electronic states often serve as active sites for activation of peroxyl bonds. Additionally, the doped heteroatoms allow for the fine-tuning of the physicochemical properties of carbon materials such as conductivity and wettability, further enhancing the catalytic performance [85-88]. For example, the high electronegativity difference between N and C (3.07 *vs.* 2.55) alters the charge distribution around the N-dopants, endowing the doped N atoms and the adjacent C atoms a highly negative and positive charge density, respectively [89]. The changes in local charge density facilitate the adsorption and subsequent activation of the peroxides. N-doped porous carbon (CNC800) was prepared by carbonizing a copolymer derived from aniline and pyrole under N_2 atmosphere at 800 °C for persulfate activation [90]. The asymmetrical electron redistribution near the pyridinic N sites favored persulfate adsorption and enabled pyridinic N sites as the mediator facilitating the electron transfer process for oxidation of the aqueous organics (Fig. 4b) [90]. Notably, the doped heteroatoms in different bonding state can impart drastically different properties to carbocatalysts and influence peroxide activation behaviors. Specifically, graphitic N located within the graphitic frameworks enhances the conductivity and stability of catalysts while the edge or defect situated pyridinic N improves electron-accepting ability of the graphitic matrix [91,92]. These two N doping sites usually play as the active sites for activation of peroxides. Pyrrolic N at the defects or vacancies, however, often hinders the electron transfer properties [93]. Heteroatom doping could be achieved by either direct/*in-situ* synthesis relying on the intrinsic heteroatoms within the molecular structures of the precursors or by post-treatment methods such as pyrolysis or annealing with external heteroatom sources. Nevertheless, precisely controlling the concentration and coordination states of the heteroatom dopants in carbocatalysts remains challenging because of the complex interactions between the metal-free dopants with the carbon surface.

Metal atoms, especially the transition metal atoms such as Fe, Ni, Co, and Mn, have also been dispersed into the skeleton of the graphitic carbons to form single-atom catalysts (SACs) for peroxides activations [9]. By downsizing the metal particles to single atom scale, the SACs maximize the exposure of metal sites by preventing their aggregations and showcase unique electronic properties [94]. Compared to conventionally metal-loaded carbocatalysts, single-dispersed atoms (SAs) in SACs feature low coordinations and unsaturated status, enhancing their intrinsic catalytic activities *via* the strong metal and support interaction (SMSI) [95]. Porous graphitic C_3N_4 (g-C_3N_4) catalysts with atomically-dispersed transition metals have been proved to be highly effective for O_3 activation [96]. Reaction pathways can differ by the types of the doped transition metals within the g-C_3N_4 skeleton by affecting the O_3 adsorption behaviors (Fig. 4c). After O_3 adsorption on the Mn_1–C_3N_4 sites with saturated coordination, it evolved into Griffiths-type coordinated $^*OO$, which further evolved into $O_3^{\bullet-}$ to produce aqueously-bound $^\bullet OH$ to attack organics. For Co_1–C_3N_4 sites with unsaturated coordination, the Pauling-type coordinated $^*OO$ was formed after O_3 was adsorbed. The unsaturated coordination of Co as well as the relatively low steric effect favored the further adsorption of organics to induce surface oxidation mechanisms. However, synthesizing SACs with high metal loadings is challenging because high metal concentrations risk aggregating the isolated atoms with high surface energy. Additionally, strong anchoring of metal atoms minimizes metal leaching and mitigates the cyclic instability of the conventional metal-loaded carbocatalysts in highly oxidizing environments produced by peroxide activation [7]. The special architecture of porous carbons with high specific surface area and tunable surface properties provides a versatile platform to integrate the single-dispersed metal atom. Graphitic C_3N_4 (g-C_3N_4) confined with atomically-dispersed Mn–N_4 (Mn–CN) sites was prepared by atom trapping from metal nanoparticles/bulk metals to activate the peroxone reaction between O_3 and H_2O_2 for oxalic acid (OA) removal [97]. Single-atom Mn–N_4 sites facilitate stable and spontaneous adsorption of H_2O_2, leading to in the formation of robust HOO–Mn–N_4 bonds. Notably, these bonds readily decompose in the presence of O_3, accelerating the production of $O_3^{\bullet-}$ and $HO_2^\bullet$, thereby facilitating the breakdown of recalcitrant organic compounds. However, synthesizing SACs with high metal loadings is challenging because high metal concentrations risk aggregating the isolated atoms with high surface energy.

In summary, introducing doped heteroatoms and defect sites serve as the universal strategies to create active sites to enhance

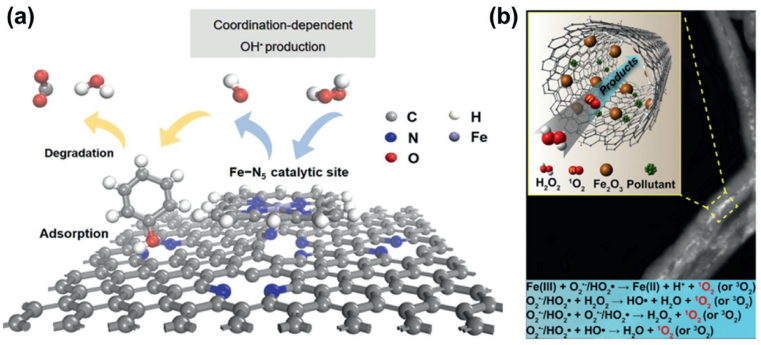

Fig. 5. (a) Axial coordination tuning Fe single-atom catalysts for boosting H_2O_2 activation. Reprinted with permission [101]. Copyright 2023, Wiley-VCH. (b) Illustration of possible mechanism of pollutants degradation in Fe_2O_3@FCNT-H/H_2O_2 system. Reprinted with permission [105]. Copyright 2019, Proc. Natl. Acad. Sci. U. S. A.

the adsorption and the subsequent activation of peroxides. Considering the different properties of the peroxides and the differences in reaction phase, the strategies in pore formation and wettability control can be different towards their activation. The involvement of gas-phase peroxides such as ozone usually requires a larger pore size to enrich the reactants than the peroxides with high aqueous solubilities. In addition, the presence of the gas-phase peroxides requires balance between the aerophilicity and the hydrophilicity of the catalyst surface to enhance the mass transfer efficiency, which calls for a much more stringent regulation of the surface wettability than the di-phase Fenton-like reactions. For triphase peroxide activation processes, it is recommended to construct the GDL reaction interface to enhance the affinities of the catalyst surface to both gas-phase peroxides and the liquid-phase contaminants.

4. Applications porous carbocatalysts in peroxides activation

4.1. Fenton/Fenton-like reaction

The covalent nature of the peroxide bond in H_2O_2, with an O–O bond length of 1.453 Å and a bond energy of 213.1 kJ/mol, makes it prone to accept electrons [98]. Cleavage of the peroxyl bond within H_2O_2 leads to the formation of highly oxidative •OH. In conventional Fe-triggered Fenton reactions, although Fe loaded onto the porous carbon matrix initiates rapid kinetics for H_2O_2 activation through single-electron transfer from Fe^{2+} to the peroxyl bond, the high activities can only be maintained within a narrow pH range (~3) [99]. The leached Fe cations under acidic environment tend to aggregate into sludges. Additionally, the sluggish reduction kinetics for Fe^{2+} regeneration ($Fe^{3+} + H_2O_2 \rightarrow Fe^{2+} + HO_2^{\bullet} + OH^+$, 0.02 mol L^{-1} s^{-1}) hinders ongoing H_2O_2 activation and decreases the oxidation efficiency [100].

To address these limitations, atomic-dispersed Fe species are doped or integrated into the porous carbon matrix [101]. As mentioned before, downsizing the metal particles to single atom scale maximizes their exposures. Furthermore, the rich porous structures further enhance the diffusion of the reactants to these atomic-dispersed Fe sites. Metal-free heteroatoms and/or co-catalysts have also been doped/integrated within the carbon skeleton and the pore structures to accelerate the reduction kinetics for Fe^{2+} regeneration [102]. In a recent study, iron phthalocyanine molecules (FePc) were integrated on N-doped graphene (NG) by a facile high temperature pyrolysis method, in which N atoms acted as anchoring sites for single atomic dispersed Fe [101]. Axially coordinated Fe atoms in Fe–N_5 sites shortened the diffusion distance of the produced •OH to interact with the adsorbed phenol. molecules on the adjacent pyridinic N sites on NG, thus substantially improving the oxidation efficacy (Fig. 5a). Additionally, the incorporated Fe species have been replaced by other transition metals such as Co, Ni and Mn to induce Fenton-like reactions relying on the redox cycles of the Fe-free transition metals [103].

Apart from enhancing the dispersion of the metal-based active sties and regulating the local electronic configurations, anchoring metal species within the ordered mesoporous structures can invoke the nanoconfinement effect, which boosts the kinetics of the Fenton/Fenton-like reactions by promoting the transportation and enrichment of reactants [104]. Pan *et al.* implanted Fe_2O_3 nanoparticles on the inner wall of multiwalled carbon nanotubes (Fe_2O_3@FCNT-H) for Fenton-like catalysis [105]. The electron-deficient concave surfaces of the inner walls of MWCNTs prompted a strong electronic interaction with the Fe_2O_3 nanoparticles, facilitating the reduction of Fe(III) by H_2O_2 to produce $HO_2^{\bullet}$ radicals. These radicals then evolved into $^1O_2$ *via* the Haber-Weiss reaction for fast degradation of organic pollutants (Fig. 5b). It was believed that the confine space within MWCNTs influences the spin state of Fe(III), thereby enhancing the reaction kinetics with H_2O_2 for $HO_2^{\bullet}$ production. Employing $^1O_2$ as the dominant ROS dramatically broadened the optimal working pH range from 5.0 to 9.0, which greatly expanded the use of Fenton-like catalysis in alkaline conditions. Table S2 (Supporting information) summarizes the recent advances in porous carbocatalysts-driven Fenton/Fenton-like reactions for oxidation of aqueous organic pollutants.

4.2. Catalytic persulfates activation

Persulfates, including peroxymonosulfate (PMS) and persulfate (PDS), are derivatives of H_2O_2, with one or both terminal H atoms of the H_2O_2 replaced by the sulfite groups (–SO_3) [106]. The elongated length of the peroxyl bonds within the persulfates (1.460 and 1.497 Å for PMS and PDS, respectively) compared to that of the H_2O_2 (1.453 Å) favors their activation by direct electron transfer mechanisms [98]. Recently, porous carbocatalysts with either metal-free active sites such as heteroatom dopants, surface functionalities, and defective structures or metal-involved active sites such as loaded metal particles, encapsulated metal species, and atomic dispersed metal species have been developed and proved to be catalytically active for persulfates activation (Table S3 in Supporting information). The intimate electronic communications between the persulfate molecules and the active sites with fine-tuned electronic properties facilitate the peroxide bonds activation to produce radical or nonradical based ROS for rapid oxidation of the organics [107]. Nevertheless, carbocatalysts dominated by the microporous structures may limit the availability of active sites. Narrowed pore size impedes the diffusion of persulfates and the organic pollutants within the carbon matrix [108].

Regulating the pore size of the carbocatalysts to foster meso/macro-pore dominated structures can significantly enhance the availability of active sites by promoting the diffusion of the re-

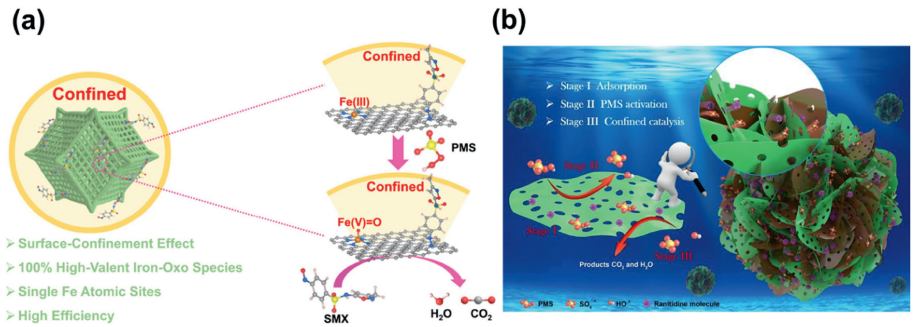

Fig. 6. (a) Mechanism of the nanoconfinement effect promoting PMS activation. Reprinted with permission [65]. Copyright 2023, American Chemical Society. (b) Schematic illustration of the mechanism of RAN degradation by BN–Co_3O_4 NC/PMS heterogeneous system. Reprinted with permission [109]. Copyright 2022, Elsevier.

actants. Xu *et al.* synthesized isolated Co atoms on tubular carbon nitride (CN) as an effective catalyst for PMS activation [86]. The tubular meso/macro-porous structure and single Co atom dispersion provide abundant active sites, enabling strong interaction with PMS and its activation intermediates and thus demonstrating high capability for PMS activation and selectivity for $^1O_2$ generation. A single Fe atom supported on mesoporous N-doped carbon was synthesized as an effective activator for PMS-AOPs (Fig. 6a) [65]. The mesopores acted as nanoreactors to enrich and restrict movement of the reactants. The confined diffusion of the reactants markedly improved the probability of contact between pollutants and active sites, improving the degradation efficiency. The collisions of the reactants can be further increased when they are confined in a proper mesoporous structure. Moreover, the altered molecular properties of the reactants by the induced nanoconfinement effect can modulate both reaction kinetics and thermodynamics and boost the oxidation efficiency. Boron nitride (BN)-Co_3O_4 nanosheet cluster can serve as a nanoconfined catalyst for PMS activation to degrade Ranitidine (RNA) [109]. The presence of the mesoporous void spaces within the catalysts significantly reduced diffusion distance for pollutants to reach the catalyst surfaces and increased the instantaneous concentration of reactants. As a result, high degradation efficiency can be achieved by the improved collision frequency of RNA and generated ROS ($^{\bullet}OH$ and $SO_4^{\bullet-}$) (Fig. 6b).

Additionally, enhancing the surface hydrophilicity of the carbocatalysts can improve the uniform interactions with reaction solution containing the dissolved persulfates and organic pollutants peroxides. Li *et al.* embedded amino-functionalized mesoporous silica onto NG sheets (NG/NH_2−MCM-41) to enhance the surface hydrophilicity of the carbocatalysts, serving as a heterogeneous PMS activation catalyst for bisphenol A (BPA) removal [110]. The hydrophilic NG/NH_2−MCM-41 composites possessed preferable dispersion and uniform interactions with reaction solution. This enabled the effective adsorption of the reactants on catalysts, accelerating the generation of $^{\bullet}OH$, $SO_4^{\bullet-}$ and $^1O_2$.

4.3. Catalytic ozonation processes

Ozone (O_3) with a high oxidation potential of 2.07 V obtains high affinity towards organics with unsaturated carbon bonds and ozonation process has been extensively used in water and wastewater treatments [111]. However, ozone is quite inert against the small molecular aliphatic acids with saturated carbon bonds, which are common degradation intermediates of the phenolic pollutants. Heterogeneous activation of the peroxide bond within the O_3 molecule can produce highly oxidative ROS such as $^{\bullet}OH$ and surface-adsorbed activated oxygen species for fast mineralization of the aliphatic acids (Fig. 7a) [16]. Similar to activation of the persulfates, extensive studies have concentrated on designing and developing porous carbocatalysts with high activity and stability (Table S4 in Supporting information). Additionally, the intrinsic active sites on carbocatalysts have been well elucidated [112]. Nevertheless, O_3 utilization efficiencies in most of the reported system are usually quite low (<20%) because of the inherent low solubility of O_3 in water and the high mass transfer resistance at the gas–liquid and liquid–solid interfaces [80]. Furthermore, the limited porosity of bulk carbons hampers the exposure of the active sites and the adsorption of the reactants. Pore construction is a potent strategy to enhance the catalytic ozonation activities of carbocatalysts by increasing the exposure of active sites and promoting mass transfer rates (Fig. 7b) [113]. Besides acting as nanoreactors to concentrate reactants, the confined spaces in pore-rich carbocatalysts can also increase the flow rate of the reaction solution, thereby elevating the diffusion of reactants and improve their interactions at the gas-liquid-solid interface (Fig. 7c) [76]. The enhanced utilization of active sites and the accelerated reaction kinetics improve the O_3 utilization efficiency. Wu *et al.* synthesized hierarchically porous carbon microspheres (HPCM-4–900) by a rapid aerosol-confined salt/surfactant templating approach for catalytic ozonation [113].

The 3D maze-like structures with vast meso/macropores act as microreactors to effectively trapped O_3 bubbles. The high local O_3 concentration at the reaction interfaces enhanced mass transfer and promoted the activation of O_3 on carbonyl group and defects to produce $O_2^{\bullet-}$ and surface-adsorbed activated ROS for degradation of organics. In addition to pore construction, the as-mentioned wettability regulation by loading hydrophilic catalysts onto the hydrophobic GDL can be employed to enhance the diffusion and utilization of O_3 by the built tri-phase mass transfer interface [82].

4.4. Catalytic activation of other peroxides

Apart from the previously discussed catalytic peroxides activation systems, emerging peroxides like percarbonates, periodate, and peroxyacetic acid have recently been activated by porous carbocatalysts to quickly degrade aqueous organic pollutants (Table S5 in Supporting information) [114-116]. Sodium percarbonate (SPC), as a solid carrier of H_2O_2, has been widely utilized to induce Fenton-like reactions because of its cost-effectiveness and transportability [117]. It is found that the irregular tubular mesoporous structures in iron-rich sludge-derived biochar promoted rapid decomposition of SPC on the Fe sites and generation of $^{\bullet}OH$ for the effective degradation of aqueous sulfamethoxazole (Fig. 8a) [118]. Activating the peroxide bonds in peroxymonocarbonate (PMC, with chemical formula of H–O–O–CO_2^-) can initiate a cascade of complex chemical reactions, generating various types of ROS such as $^{\bullet}OH$, $^{\bullet}O_2^-$, $CO_3^{\bullet-}$, and $^1O_2$ [116,119]. Moreover, the produced bicarbonate from percarbonates acts as a buffer to reduce the leaching of the doped metal species. AOPs based on periodate (PI) activation are promising treatment technologies due to the high oxidative potentials of generated active species (*i.e.*, $IO_3^{\bullet}$, $IO_4^{\bullet}$, $^{\bullet}OH$, $O_2^{\bullet-}$, $^1O_2$) and the produced iodate as an environmentally friendly byproduct [120]. Studies have revealed that active species generated within

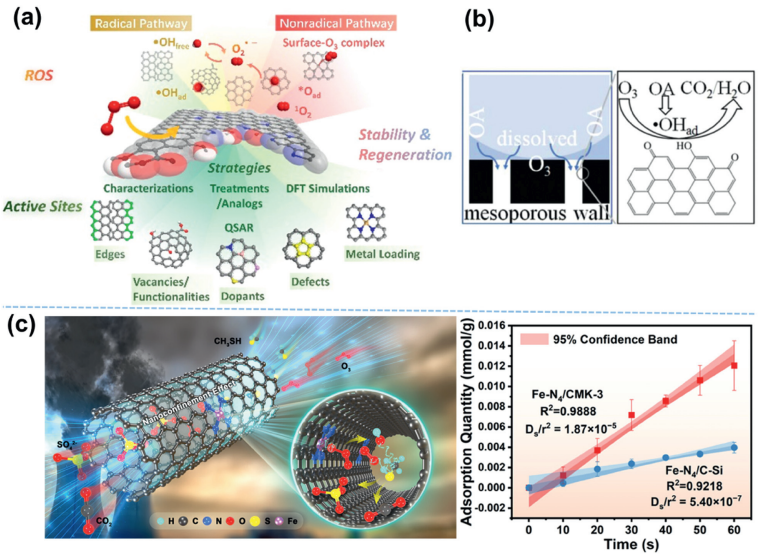

Fig. 7. (a) Design strategies of carbocatalysts for catalytic ozonation. Reprinted with permission [16]. Copyright 2020, American Chemical Society. (b) Schematic illustration for the catalytic ozonation of oxalate on HPCM-4–900. Reprinted with permission [113]. Copyright 2024, Wiley-VCH. (c) Schematic illustration of nanoconfinement effect for enhancing the CH_3SH removal efficiency and O_3 diffusion coefficient for confined system Fe–N_4/CMK-3 and unconfined system Fe–N_4/C–Si. Reprinted with permission [76]. Copyright 2023, American Chemical Society.

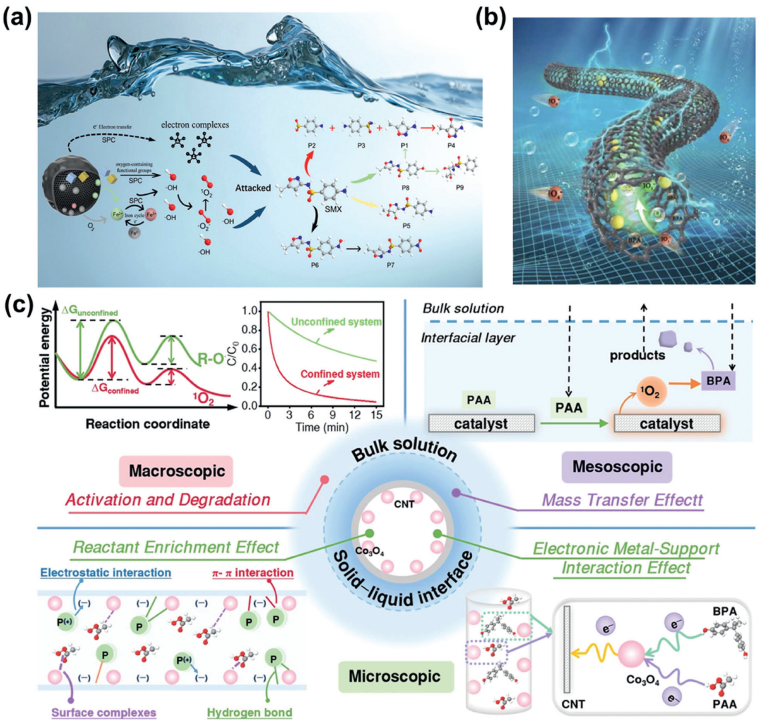

Fig. 8. (a) The possible mechanism of SMX degradation in the Fe-BC/SPC process. Reprinted with permission [118], Copyright 2023, Elsevier. (b) Schematic illustration of possible mechanism of pollutants degradation in Fe_2O_3-in-CNT/PI systems. Reprinted with permission [114], Copyright 2022, Wiley-VCH. (c) The intrinsic principles of PAA activation in confined systems from macroscopic, mesoscopic to microscopic dimensions. Reprinted with permission [115], Copyright 2023, Nature.

the confined spaces of porous carbocatalysts during PI activation can differ significantly from those in open spaces (Fig. 8b) [114]. Peracetic acid (PAA) has emerged as a promising disinfectant in wastewater, owing to its high redox potential (1.06-1.96 V) and a relatively weak O–O bond (159 kJ/mol), which can be easily activated to generate reactive species [121]. Zhang *et al.* prepared catalysts with Co_3O_4 encapsulated inside CNTs (Co_3O_4-in-CNT) and loaded on the outside of CNTs (Co_3O_4-out-CNT) for PAA activation (Fig. 8c) [115]. Co_3O_4-in-CNT and Co_3O_4-out-CNT could initiate distinct PAA activation mechanisms. For Co_3O_4-out-CNT, PAA activation occurred through the redox cycling of Co, leading to the generation of R-O$^{\bullet}$ radicals, including $CH_3C(O)O^{\bullet}$ and $CH_3C(O)OO^{\bullet}$. On the other hand, Co_3O_4-in-CNT triggered PAA activation *via* a non-radical mechanism by generating $^1O_2$.

5. Conclusions and outlook

Porous carbocatalysts with high specific surface area, tunable pore size, and programmable active sites demonstrate outstanding performance in activation of peroxides to generate active species for treatment of aqueous organic pollutants. This review summarizes pore construction methods, including physi-

cal/chemical activations and employing sacrificial templates. Engineering strategies to enhance the activities of the porous carbocatalysts towards activation of the peroxides are outlined. Constructing meso/macroporous structures facilitates the diffusion of the reactants within the carbocatalysts. Controlling the wettability of the carbocatalysts is crucial for tuning the interactions between the reactants and the surface of the carbocatalysts. Defect engineering induces alterations in charge distribution and optimizing the electronic properties around the active sites, contributing to the high activities. Lastly, the applications of the engineered porous carbocatalysts in various peroxide activation systems are critical summarized. Although remarkable progress has been made in the development of porous carbocatalysts and the exploration of the mechanisms in peroxides activation, there remain both challenges and opportunities in enhancing their activities and extending their possible practical applications.

(1) Improper removal of the template for pore constructions may impact the microstructure of material and alter the surface chemical properties and thus affecting the catalytic performance. Careful selection of the washing solvents and chemical etchants and precise control of heat treatment conditions are imperative during the template removal.
(2) The precise enrichment of the reactants within the nanoconfined spaces rather than adsorbed on external surfaces remains a technical challenge. It is crucial to regulate the interactions by enhancing their electrostatic attraction and tuning the wettability to promote mass transfer efficiency.
(3) Precisely controlling the concentration and coordination states of the heteroatom dopants (both metal-based and metal-free) in carbocatalysts is challenging. Advanced synthesis techniques such as atomic layer deposition (ALD), chemical vapor deposition (CVD), and radiation doping can be employed to fine-tune the concentrations of the dopants and microenvironment of the coordination.

Declaration of competing interest

The authors declare no competing financial interests or personal relationships that could have appeared to influence the work reported in this paper.

CRediT authorship contribution statement

Bofeng Li: Writing – original draft, Investigation. **Yuxian Wang:** Writing – review & editing. **Ya Liu:** Investigation. **Zhe Han:** Investigation. **Tiantian Xing:** Investigation. **Yumin Zhang:** Investigation. **Chunmao Chen:** Supervision.

Acknowledgments

The authors greatly appreciate the financial supports from the National Natural Science Foundation of China (Nos. 22478426 and 22278436), Young Elite Scientists Sponsorship Program by BAST (No. 1101020370359), and Science Foundation of China University of Petroleum, Beijing (No. 2462021QNXZ009).

Supplementary materials

Supplementary material associated with this article can be found, in the online version, at doi:10.1016/j.cclet.2024.110374.

References

[1] D.B. Miklos, C. Remy, M. Jekel, et al., Water Res. 139 (2018) 118–131.
[2] C. Nie, J. Wang, B. Cai, et al., Appl. Catal. B: Environ. 340 (2024) 123173.
[3] H. Wang, S. Zhang, X. He, et al., Chem. Eng. J. 452 (2023) 139503.
[4] H. Huang, M. Zhang, K. Xu, et al., Chem. Eng. J. 484 (2024) 149595.
[5] Y. Liu, C. Chen, X. Duan, et al., J. Mater. Chem. A 9 (2021) 18994–19024.
[6] H. Sun, Z. Yan, F. Liu, et al., Adv. Mater. 32 (2020) 1806326.
[7] Y. Gao, T. Wu, C. Yang, et al., Angew. Chem. Int. Ed. 60 (2021) 22513–22521.
[8] X. Duan, H. Sun, S. Wang, Acc. Chem. Res. 51 (2018) 678–687.
[9] Y. Shang, X. Xu, B. Gao, et al., Chem. Soc. Rev. 50 (2021) 5281–5322.
[10] J. Dai, H. Zhang, Small 17 (2021) 2005334.
[11] S. Zhang, L. Chen, Z. Qu, et al., Chem 9 (2023) 3172–3184.
[12] H. Du, X. Zhang, L. Ding, et al., Catal. B: Environ. 342 (2024) 123396.
[13] L. Li, L. Xu, Z. Hu, et al., Adv. Funct. Mater. 31 (2021) 2106120.
[14] C. Chu, J. Yang, D. Huang, et al., Environ. Sci. Technol. 53 (2019) 10352–10360.
[15] C. Zheng, X. Cheng, C. Yang, et al., RSC Adv. 5 (2015) 98842–98852.
[16] Y. Wang, X. Duan, Y. Xie, et al., ACS Catal. 10 (2020) 13383–13414.
[17] Q. Li, C. Chen, C. Li, et al., ACS Nano 14 (2020) 13652–13662.
[18] Y. Jiang, J. Wang, B. Liu, et al., Chem. Eng. J. 446 (2022) 137361.
[19] D. Wakerley, S. Lamaison, J. Wicks, et al., Nat. Energy 7 (2022) 130–143.
[20] H. Chang, X. Liu, S. Zhao, et al., Adv. Funct. Mater. 34 (2023) 2313491.
[21] R. Guo, X. Hu, X. Chen, et al., Small 19 (2023) 2207767.
[22] D.V. Cuong, B.M. Matsagar, M. Lee, et al., Renew. Sustain. Energy Rev. 145 (2021) 111029.
[23] B. Zdravkov, J. Čermák, M. Šefara, et al., Open Chem. 5 (2007) 385–395.
[24] Z. Tang, X. Li, L. Tong, et al., Angew. Chem. Int. Ed. 60 (2021) 23608–23613.
[25] W. Schwieger, A.G. Machoke, T. Weissenberger, et al., Chem. Soc. Rev. 45 (2016) 3353–3376.
[26] H. Teng, S. Wang, Carbon 38 (2000) 817–824.
[27] S.M. Hong, S.W. Choi, S.H. Kim, K.B. Lee, Carbon 99 (2016) 354–360.
[28] I. Moulefera, F.J. García Mateos, A. Benyoucef, et al., Front. Mater. 7 (2020) 153.
[29] J. Lee, J. Kim, T. Hyeon, Adv. Mater. 18 (2006) 2073–2094.
[30] Y. Li, G. Wang, T. Wei, Z. Fan, P. Yan, Nano Energy 19 (2016) 165–175.
[31] B. Li, Q. Cao, Y. Liu, et al., J. Mater. Chem. A 10 (2022) 24905–24914.
[32] C. Yang, H. Noguchi, K. Murata, et al., Adv. Mater. 17 (2005) 866–870.
[33] D. Qiu, N. Guo, A. Gao, et al., Electrochim. Acta 294 (2019) 398–405.
[34] L. Mo, S. Jia, S. Lin, et al., Int. J. Energy Res. 46 (2022) 2373–2384.
[35] M. Sevilla, N. Díez, A.B. Fuertes, ChemSusChem 14 (2021) 94–117.
[36] S. Yu, N. Sun, L. Hu, et al., J. Power Sources 405 (2018) 132–141.
[37] S. Tian, J. Dai, Y. Jiang, et al., J. Colloid Interface Sci. 505 (2017) 858–869.
[38] X. Zhao, P. Gao, B. Shen, et al., Renew. Sustain. Energy Rev. 188 (2023) 113808.
[39] J. Yin, W. Zhang, N.A. Alhebshi, et al., Small Methods 4 (2020) 1900853.
[40] P. Chen, M. Zhou, Y. Liu, et al., Appl. Catal. B: Environ. 346 (2024) 123767.
[41] Y. Shi, J. Huang, L. Chen, et al., J. Hazard. Mater. 424 (2022) 127465.
[42] X. Li, L. Zhao, T. He, et al., J. Power Sources 521 (2022) 230943.
[43] W. Chu, K. Wang, H. Li, et al., Chem. Eng. J. 430 (2022) 133112.
[44] S. Rehman, S. Guo, Y. Hou, Adv. Mater. 28 (2016) 3167–3172.
[45] L. Wang, P. Tang, J. Liu, et al., J. Colloid Interface Sci. 554 (2019) 260–268.
[46] X. Lu, H. Xu, P. Yang, et al., Appl. Catal. B: Environ. 313 (2022) 121454.
[47] K. Hayat, D. Bahamon, L.F. Vega, et al., ACS Appl. Mater. Interfaces 15 (2023) 54432–54445.
[48] Y. Hu, C. Chen, T. Shen, et al., Adv. Sci. 9 (2022) e2205299.
[49] A. Xie, J. Dai, Y. Chen, et al., Adv. Powder Technol. 30 (2019) 170–179.
[50] P. Ren, D. Wu, T. Wang, et al., J. Power Sources 532 (2022) 231072.
[51] W. Wang, W. Chen, P. Miao, et al., ACS Catal. 7 (2017) 6144–6149.
[52] M. Chen, S. Jiang, S. Cai, et al., Chem. Eng. J. 313 (2017) 404–414.
[53] L. Zhang, L. Jin, B. Liu, et al., Front. Chem. 7 (2019) 22.
[54] Y. Yu, W. Xu, J. Fang, et al., Appl. Catal. B: Environ. 268 (2020) 118751.
[55] Y. Mai, A. Eisenberg, Chem. Soc. Rev. 41 (2012) 5969–5985.
[56] L. Wang, Q. Li, Adv. Funct. Mater. 26 (2016) 10–28.
[57] T. Yao, J. Song, Y. Hong, et al., J. Chromatogr. A 1705 (2023) 464202.
[58] Z. Wu, W. Wu, W. Liu, et al., Angew. Chem. Int. Ed. 51 (2013) 14009–14013.
[59] H. Zhang, J. Gu, Y. Jiang, et al., Energy Convers. Manage. 86 (2014) 605–613.
[60] A. Daifullah, B. Girgis, Water Res. 32 (1998) 1169–1177.
[61] H. Zhu, X. Liu, Y. Jiang, et al., Chem. Eng. J. 422 (2021) 130584.
[62] Y. Chen, G. Zhang, H. Liu, J. Qu, Angew. Chem. Int. Ed. 58 (2019) 8134–8138.
[63] T. Ba, C. Wang, Q. Feng, et al., J. Water Process Eng. 53 (2023) 103716.
[64] K. Huang, H. Zhang, Environ. Sci. Technol. 53 (2019) 12610–12620.
[65] B. Huang, Z. Wu, X. Wang, et al., Environ. Sci. Technol. 57 (2023) 15667–15679.
[66] K. Zhou, Z. Xu, Nano Lett. 20 (2020) 8392–8398.
[67] R. Brilmayer, S. Kübelbeck, A. Khalil, et al., Adv. Mater. Interfaces 7 (2020) 1901914.
[68] J.H. Bae, J.H. Han, T.D. Chung, Phys. Chem. Chem. Phys. 14 (2012) 448–463.
[69] X. Duan, Z. Ao, H. Sun, et al., ACS Appl. Mater. Interfaces 7 (2015) 4169–4178.
[70] S. Zhang, M. Sun, T. Hedtke, et al., Environ. Sci. Technol. 54 (2020) 10868–10875.
[71] J. Sun, T. Wu, Z. Liu, et al., J. Cleaner Prod. 346 (2022) 131143.
[72] C. Cai, S. Kang, X. Xie, et al., J. Hazard. Mater. 399 (2020) 122979.
[73] Y. Ma, H. Wang, X. Lv, et al., Chem. Eng. J. 443 (2022) 136495.
[74] X. Gao, Z. Yang, W. Zhang, B. Pan, Nat. Commun. 15 (2024) 2808.
[75] S. Zhang, X. Quan, D. Wang, Environ. Sci. Technol. 52 (2018) 8701–8711.
[76] W. Qu, M. Luo, Z. Tang, et al., Environ. Sci. Technol. 57 (2023) 13205–13216.
[77] J. Yang, Q. Peng, Y. Xu, et al., ACS Appl. Mater. Interfaces 15 (2023) 45441–45454.
[78] P. Wang, J. Zhao, R. Shi, et al., Mater. Today Energy 23 (2022) 100908.
[79] J. Yu, W. Chen, K. Li, et al., Angew. Chem. Int. Ed. 134 (2022) e202207255.
[80] L. Magi, F. Schweitzer, C. Pallares, et al., J. Phys. Chem. A 101 (1997) 4943–4949.

[81] Z. Wang, K. Li, J. Guo, et al., Environ. Sci. Technol. 57 (2023) 18647–18657.
[82] H. Rabiee, L. Ge, X. Zhang, et al., Energy Environ. Sci. 14 (2021) 1959–2008.
[83] F. Banhart, J. Kotakoski, A.V. Krasheninnikov, ACS Nano 5 (2011) 26–41.
[84] Q. Wu, X. Yan, Y. Jia, X. Yao, EnergyChem 3 (2021) 100059.
[85] P. Cao, X. Quan, K. Zhao, et al., Environ. Sci. Technol. 54 (2020) 12662–12672.
[86] Z. Wang, E. Almatrafi, H. Wang, et al., Angew. Chem. Int. Ed. 134 (2022) e202202338.
[87] Y.G. Lee, J. Lee, G.H. An, Adv. Funct. Mater. 31 (2021) 2104256.
[88] C. Nie, Z. Dai, W. Liu, et al., Environ. Sci.: Nano 7 (2020) 1899–1911.
[89] L.C. Allen, J. Am. Chem. Soc. 111 (1989) 9003–9014.
[90] K. Silambarasan, A.V. Narendra Kumar, W.S. Shin, Chem. Eng. J. 474 (2023) 145922.
[91] Z. Lin, Y. Yang, M. Li, et al., Angew. Chem. Int. Ed. 58 (2019) 16973–16980.
[92] G. Qu, P. Jia, S. Tang, et al., J. Hazard. Mater. 461 (2024) 132626.
[93] Y. Wang, Z. Zhang, Z. Yin, et al., Appl. Catal. B: Environ. 319 (2022) 121891.
[94] Q. Jin, W. Liu, Y. Dong, et al., J. Cleaner Prod. 423 (2023) 138688.
[95] T. Cui, L. Li, C. Ye, et al., Adv. Funct. Mater. 32 (2022) 2108381.
[96] J. Wang, Y. Xie, G. Yu, et al., Environ. Sci. Technol. 56 (2022) 17753–17762.
[97] Z. Guo, Y. Xie, J. Xiao, et al., J. Am. Chem. Soc. 141 (2019) 12005–12010.
[98] V. Hasija, V.H. Nguyen, A. Kumar, et al., J. Hazard. Mater. 413 (2021) 125324.
[99] K. Datta, M. Gawande, K. Datta, et al., J. Mater. Chem. A 4 (2016) 596–604.
[100] J. Lin, W. Tian, Z. Guan, et al., Adv. Funct. Mater. 32 (2022) 2201743.
[101] H. Fu, J. Wei, G. Chen, et al., Appl. Catal. B: Environ. 321 (2023) 122012.
[102] C. Zhou, P. Zhou, M. Sun, et al., Water Res. 210 (2022) 117984.
[103] Y. Yao, S. Wang, C. Wang, et al., J. Mater. Chem. A 12 (2024) 10081–10089.
[104] W. Gu, X. Huang, Y. Tian, et al., Appl. Surf. Sci. 538 (2021) 147813.
[105] Z. Yang, J. Qian, A. Yu, et al., Proc. Natl. Acad. Sci. U. S. A. 116 (2019) 6659–6664.
[106] C. Nie, Z. Dai, L. Wan, et al., ACS ES&T Water 3 (2023) 3004–3014.
[107] B. Li, Y. Liu, K. Hu, et al., Adv. Funct. Mater. 34 (2024) 2401397.
[108] L. Hao, J. Zhang, J. Liu, et al., Chem. Rec. 23 (2023) e202300203.
[109] Y. Ma, B. Ji, X. Lv, et al., Chem. Eng. J. 435 (2022) 135126.
[110] B. Zhang, T. Wu, D. Sun, et al., Carbon 147 (2019) 312–322.
[111] H. Wang, J. Zhan, W. Yao, et al., Water Res. 130 (2018) 127–138.
[112] J. Yu, L. Tang, Y. Pang, et al., Appl. Catal. B: Environ. 260 (2020) 118160.
[113] C. Li, Z. Hu, G. Jiang, Y. Zhang, Z. Wu, Small 20 (2024) 2305316.
[114] D. Guo, Y. Yao, S. You, et al., Appl. Catal. B: Environ. 309 (2022) 121289.
[115] T. Liu, S. Xiao, N. Li, et al., Nat. Commun. 14 (2023) 2881.
[116] B. Zhang, L. Kuang, Y. Teng, M. Fan, Y. Ma, J. Environ. Sci. 105 (2021) 100–115.
[117] C. Zhang, Y. Dong, B. Li, et al., J. Cleaner Prod. 177 (2018) 245–253.
[118] Z. Mo, Z. Tan, J. Liang, et al., Chem. Eng. J. 457 (2023) 141150.
[119] L. Pi, N. Yang, W. Han, et al., Chem. Eng. J. 334 (2018) 1297–1308.
[120] R. Li, J. Wang, H. Wu, et al., Sep. Purif. Technol. 292 (2022) 120928.
[121] T. Zhang, C. Huang, Environ. Sci. Technol. 54 (2020) 7579–7590.